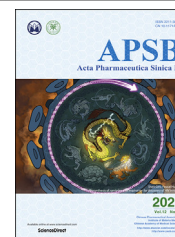




Chinese Pharmaceutical Association
Institute of Materia Medica, Chinese Academy of Medical Sciences

Acta Pharmaceutica Sinica B

www.elsevier.com/locate/apsb
www.sciencedirect.com



ORIGINAL ARTICLE

Novel dual inhibitor for targeting PIM1 and FGFR1 kinases inhibits colorectal cancer growth *in vitro* and patient-derived xenografts *in vivo*



Fanxiang Yin^{a,b,c,†}, Ran Zhao^{a,b,†}, Dhilli Rao Gorja^b, Xiaorong Fu^{a,b},
Ning Lu^{a,b}, Hai Huang^b, Beibei Xu^{a,b}, Hanyong Chen^d,
Jung-Hyun Shim^e, Kangdong Liu^{a,b,f}, Zhi Li^g, Kyle Vaughn Laster^b,
Zigang Dong^{a,b,d,*}, Mee-Hyun Lee^{a,b,h,*}

^aDepartment of Pathophysiology, School of Basic Medical Sciences, Zhengzhou University, Zhengzhou 450001, China

^bChina-US (Henan) Hormel Cancer Institute, Zhengzhou 450008, China

^cTranslational Medical Center, the First Affiliated Hospital of Zhengzhou University, Zhengzhou 450052, China

^dThe Hormel Institute, University of Minnesota, Austin, MN 55912, USA

^eDepartment of Biomedicine, Health & Life Convergencence Science, BK21 Four, College of Pharmacy, Mokpo National University, Jeonnam 58554, Republic of Korea

^fThe Collaborative Innovation Center of Henan Province for Cancer Chemoprevention, Zhengzhou 450001, China

^gDepartment of General Surgery, the Affiliated Tumor Hospital of Zhengzhou University, Zhengzhou 450008, China

^hCollege of Korean Medicine, Dongshin University, Naju 58245, Republic of Korea

Received 26 March 2022; received in revised form 15 May 2022; accepted 24 May 2022

KEY WORDS

PIM1;
FGFR1;
Colorectal cancer;
HCI-48;
Targeted therapy;
Small molecule compound
of chalcone;
Patient-derived xenograft

Abstract Colorectal cancer (CRC) is the second most common cause of cancer-related death in the world. The pro-viral integration site for Moloney murine leukemia virus 1 (PIM1) is a proto-oncogene and belongs to the serine/threonine kinase family, which are involved in cell proliferation, migration, and apoptosis. Fibroblast growth factor receptor 1 (FGFR1) is a tyrosine kinase that has been implicated in cell proliferation, differentiation and migration. Small molecule HCI-48 is a derivative of chalcone, a class of compounds known to possess anti-tumor, anti-inflammatory and antibacterial effects. However, the underlying mechanism of chalcones against colorectal cancer remains unclear. This study reports that HCI-48 mainly targets PIM1 and FGFR1 kinases, thereby eliciting antitumor effects on colorectal cancer

*Corresponding authors. Tel.: +86 371 65587008; fax: +86 371 65587670.

E-mail addresses: zgdong@hci-cn.org (Zigang Dong), mhyun_lee@hanmail.net (Mee-Hyun Lee).

[†]These authors made equal contributions to this work.

Peer review under responsibility of Chinese Pharmaceutical Association and Institute of Materia Medica, Chinese Academy of Medical Sciences.

<https://doi.org/10.1016/j.apsb.2022.07.005>

2211-3835 © 2022 Chinese Pharmaceutical Association and Institute of Materia Medica, Chinese Academy of Medical Sciences. Production and hosting by Elsevier B.V. This is an open access article under the CC BY-NC-ND license (<http://creativecommons.org/licenses/by-nc-nd/4.0/>).

model;
Kinase activity

growth *in vitro* and *in vivo*. HCI-48 inhibited the activity of both PIM1 and FGFR1 kinases in an ATP-dependent manner, as revealed by computational docking models. Cell-based assays showed that HCI-48 inhibited cell proliferation in CRC cells (HCT-15, DLD1, HCT-116 and SW620), and induced cell cycle arrest in the G2/M phase through modulation of cyclin A2. HCI-48 also induced cellular apoptosis, as evidenced by an increase in the expression of apoptosis biomarkers such as cleaved PARP, cleaved caspase 3 and cleaved caspase 7. Moreover, HCI-48 attenuated the activation of downstream components of the PIM1 and FGFR1 signaling pathways. Using patient-derived xenograft (PDX) murine tumor models, we found that treatment with HCI-48 diminished the PDX tumor growth of implanted CRC tissue expressing high protein levels of PIM1 and FGFR1. This study suggests that the inhibitory effect of HCI-48 on colorectal tumor growth is mainly mediated through the dual-targeting of PIM1 and FGFR1 kinases. This work provides a theoretical basis for the future application of HCI-48 in the treatment of clinical CRC.

© 2022 Chinese Pharmaceutical Association and Institute of Materia Medica, Chinese Academy of Medical Sciences. Production and hosting by Elsevier B.V. This is an open access article under the CC BY-NC-ND license (<http://creativecommons.org/licenses/by-nc-nd/4.0/>).

1. Introduction

Colorectal cancer (CRC) is the second most common cause of cancer death worldwide¹. In China, the incidence of colorectal cancer has been increasing, which is common in western nations^{2,3}. Numerous studies have shown that CRC morbidity and mortality are closely related to the following factors: genetic variants⁴, race⁵, family⁶, age^{7,8}, high fat intake^{9,10}, red meat consumption, obesity¹¹, alcohol consumption, smoking^{12,13} and physical inactivity^{14,15}. Currently, surgery and chemotherapy are the main methods used for treatment of colorectal cancer¹⁶. Surgical treatment is suitable for patients diagnosed at early stages. However, nearly 60%–70% of confirmed cases in symptomatic patients are detected at later stages¹⁷. Despite the use of an active clinical treatment regimen¹⁸, the prognosis of patients with advanced colorectal cancer still remains poor due to metastasis^{19–21}. Therefore, it is urgent to find effective drug preparations and develop new therapeutic strategies to improve the prognosis of colorectal cancer.

PIM1 (proviral integration site for Moloney murine leukemia virus 1), a proto-oncogene, encodes a serine/threonine kinase. As a member of the PIM family²², it plays a crucial role in tumorigenesis, particularly in colorectal cancer²³, prostate cancer²⁴, breast cancer²⁵, glioblastoma²⁶ and lung cancer²⁷ by directly regulating the activities of various proteins involved in cell proliferation, migration and survival²⁸. Based on these facts, targeting PIM1 may be a reasonable strategy for anticancer drug development.

FGFR (fibroblast growth factor receptor) 1 is a receptor tyrosine kinase that regulates cellular processes including proliferation, survival, migration and differentiation^{29,30}. A preclinical study showed that over-expression of FGFR1 is associated with increased cancer cell proliferation and invasion³¹. In addition, the over-expression of FGFR1 or mutations of FGFR1 which lead to constitutive activation are related to the occurrence and development of hepatocellular carcinoma³², lung cancer³³, osteosarcoma³⁴ and breast cancer^{35,36}. However, it is still unclear how the regulation of PIM1/FGFR1 contributes to colorectal cancer progression. Therefore, we examined the regulatory effects and mechanisms of PIM1/FGFR1 in CRC.

Natural chalcone compounds are widely distributed in the plant kingdom^{37,38} and have a variety of biological activities³⁹, including anti-cancer⁴⁰, anti-inflammatory^{41,42}, anti-bacterial⁴³, anti-HIV⁴⁴, anti-oxidant⁴⁵ and anti-allergic activities⁴⁶. In recent years, studies

have found that chalcone is an effective chemoprophylaxis drug^{47,48} which possesses antioxidant effects and can induce apoptosis with minimal cytotoxicity^{49,50}. The activity of many chalcone compounds was measured in our previous study and compound HCI-48, a novel synthetic indole derivative of chalcone with the optimal IC₅₀ value of those compounds screened, was identified (Supporting Information Table S1). The purpose of this study was to clarify the molecular mechanism of HCI-48 in CRC and test this compound in the targeted therapy of cancer. We determined the inhibitory effect of HCI-48 by kinase profiling analysis and found that HCI-48 was inhibitory to PIM1 and FGFR1.

We hypothesized that HCI-48 could inhibit the growth of CRC by directly prohibiting PIM1 and FGFR1 kinase activities and their downstream signaling pathways *in vitro* and in PDX tumors which were over-expressing PIM1 and FGFR1.

2. Materials and methods

2.1. Reagents and materials

Compound HCI-48 (molecular weight of 394.43, purity > 95%) was synthesized by China-US (Henan) Hormel Cancer Institute (Supporting Information Fig. S1A) and the structure was identified using nuclear magnetic resonance (NMR) spectroscopy (Fig. S1B)⁵¹. Active PIM1 kinase was purchased from Millipore (Billerica, MA, USA), the recombinant BAD protein, active FGFR1, and inactive poly (Glu, Tyr) peptide for kinase assays were obtained from SignalChem Biotech Inc. (Richmond, BC, Canada). Primary antibodies for the following proteins were purchased from Cell Signaling Technology (Danvers, MA, USA): BAD (1:1000), phosphorylated BAD (*p*-BAD, 1:1000), P21 (1:1000), P27 (1:1000), phosphorylated FGFR (*p*-FGFR, 1:1000), FGFR1 (1:1000), STAT3 (1:1000), phosphorylated STAT3 (*p*-STAT3, 1:1000), AKT (1:1000), phosphorylated AKT (*p*-AKT, 1:1000), cyclin A2 (1:1000), PARP (1:1000) and cleaved PARP (1:1000), caspase 3 (1:1000), cleaved caspase 3 (1:1000), caspase 7 (1:1000), cleaved caspase 7 (1:1000), phosphorylated Histone H3 (*p*-Histone H3, 1:1000). Anti-PIM1 (1:1000) was obtained from Abcam (Cambridge, UK). Histone H3 (1:2000) was purchased from Santa Cruz Biotechnology, Inc. (Carpinteria, CA, USA). Mouse anti- β -actin antibody (1:5000), goat anti-rabbit antibody (1:5000) and goat anti-mouse antibody (1:5000) were purchased from ZSGB-Bio

Company (Beijing, China). Biotin-conjugated goat anti-rabbit (1:5000) and mouse IgG (1:5000) were purchased from Zhongshan Jinqiao Company (Beijing, China).

2.2. Cell culture and transfection

The human immortalized normal colon cell line CCD-18Co and human colorectal cancer cell lines (HCT-15, DLD1, HCT-116, SW620, HT-29 and SW480) were purchased from American Type Culture Collection (Manassas, VA, USA). Cells were cultured in minimum essential medium (MEM) (CCD-18Co and lenti-x-293T), RPMI-1640 (HCT-15 and DLD1), McCoy's 5A (HCT-116 and HT-29) or L-15 (SW620 and SW480) medium containing penicillin (100 units/mL), streptomycin (100 µg/mL), sodium pyruvate (100 mmol/L) and 10% fetal bovine serum (FBS, Biological Industries, Kibbutz Beit-Haemek, Israel). All cells were maintained at 5% CO₂ and 37 °C in a humidified incubator. All cells were cytogenetically tested and authenticated before the cells were frozen. Each vial of frozen cells was thawed and maintained in culture for a maximum of 8 weeks.

For knocking down the expression of PIM1 and FGFR1 in CRC cells, transfection was performed with *pLKO.1-MOCK*, *shPIM1* or *shFGFR1* plasmids together with packaging vectors, *pMD2.0G* and *psPAX2* (Addgene Inc., Cambridge, MA, USA) into lenti-x-293T cells using the X-Fect transfection reagent (Takara Bio, Otsu, Japan) following the manufacturer's protocols. The transfection medium was changed at 24 h after transfection. After 24 h, the virus-containing media was harvested by filtration using a 0.45 µm syringe filter and then applied to HCT-116 and SW620 cells together with 8 µg/mL of polybrene (Millipore) for 24 or 48 h. Cells were then treated with puromycin to select PIM1 or FGFR1 knock-down cells.

2.3. In vitro kinase assay

A PIM1 kinase assay was performed according to the manufacturer's instructions. Briefly, reactions were carried out in 1 × kinase buffer (25 mmol/L Tris-HCl pH 7.5, 5 mmol/L β-glycerophosphate, 2 mmol/L dithiothreitol, 0.1 mmol/L Na₃VO₄, 10 mmol/L MgCl₂, and 5 mmol/L MnCl₂) containing 100 mol/L ATP at 30 °C for 30 min. Reactions were stopped with 6 × SDS loading buffer (7 mL 4 × Tris-Cl/SDS, pH 6.8, 3 mL glycerol, 1 g SDS, 0.93 g dithiothreitol, 1.2 mg bromphenol blue, and 10 mL H₂O) and proteins were detected by immunoblotting. Active FGFR1 kinase and inactive poly (Glu, Tyr) peptide substrate were mixed in 1 × reaction buffer and then added to a white 96-well plate. Pure ATP provided in the ADP-Glo Kinase Assay (Promega, Madison, WI, USA) was serially diluted to obtain a final concentration of 10 µmol/L. HCl-48 (7.5, 15, 31 and 62.5 µmol/L) stocks were then added to reach a final concentration of 0.3, 0.6, 1.25 or 2.5 µmol/L; dimethyl sulfoxide (DMSO) was used as a control. After incubation at room temperature for 40 min, kinase activity was measured using the Luminoskan Ascent plate reader (Thermo-Scientific, Swedesboro, NJ, USA) following the protocol of ADP-Glo Kinase Assay (Promega).

2.4. In vitro and ex vivo pull-down assay

HCl-48-Sepharose 4B or DMSO-Sepharose 4B beads were prepared following the manufacturer's instructions (GE Healthcare Bio-Science, Uppsala, Sweden). 2 mg HCl-48 or DMSO and 0.3 g CNBr Sepharose 4B beads were activated by HCl (1 mL, 1 mmol/L)

and rotated at 4 °C for 24 h. Beads were then washed with 5 mL coupling buffer for a total of 5 times. Next, 5 mL 0.1 mol/L Tris·HCl buffer (pH 8.0) was added before rotating at 4 °C for 24 h. After 24 h, beads were washed by rotating at 4 °C for 5 min using 0.1 mol/L acetate (pH 4.0) buffer and centrifugation at 4 °C for 5 min. The supernatant was removed and the beads washed with 0.1 mol/L Tris·HCl with 0.5 mol/L NaCl (pH 8.5), alternatively washed by 0.1 mol/L acetate (pH 4.0) buffer and 0.1 mol/L Tris·HCl with 0.5 mol/L NaCl (pH 8.5) for 5 times, and 1 mL PBS was added. Cell lysates (500 µg) or recombinant human PIM1/FGFR1 protein (200 ng) were incubated with 100 µL HCl-48-Sepharose 4B beads or Sepharose 4B beads only in 1 × lysis buffer (50 mmol/L Tris-HCl, pH 7.5, 5 mmol/L EDTA, 150 mmol/L NaCl, 1 mmol/L dithiothreitol, 0.01% NP-40, and 2 mg/mL bovine serum albumin) at 4 °C with rotation overnight. After incubation, the beads were washed for three times with washing buffer (50 mmol/L Tris-HCl, pH 7.5, 5 mmol/L EDTA, 150 mmol/L NaCl, 1 mmol/L dithiothreitol and 0.01% NP-40). The binding of PIM1 and FGFR1 proteins to the beads was detected by Western blot after elution with 6 × SDS loading buffer at 95 °C for 5 min. For the ATP competitive binding assay, active PIM1 and FGFR1 were incubated with HCl-48-Sepharose 4B beads and 0, 10, 100, or 1000 µmol/L ATP, following the procedure described above for the binding assay.

2.5. Computational docking and modeling

To confirm that HCl-48 can bind with PIM1 and FGFR1, we performed an *in silico* docking prediction using the Schrödinger Suite 2017 software program⁵². The PIM1 and FGFR1 crystal structures were downloaded from the protein data bank and then prepared using the standard procedures of the Protein Preparation Wizard (Schrodinger Suite 2017). Hydrogen atoms were added to give a consistent pH of 7 and all water molecules were removed. The ATP-binding site-based receptor grid was generated for docking. HCl-48 was prepared for docking by default parameters using the LigPrep program. Next, the docking of HCl-48 with PIM1 and FGFR1 were accomplished with default parameters under the extra precision (XP) mode using the program Glide.

2.6. MTT cell proliferation assay

Cells were cultured and seeded (2 × 10³ cells/well for HCT-15, HCT-116 and HT-29; 1 × 10³ cells/well for DLD1; 4 × 10³ cells/well for SW620 and SW480) in 96-well plates and incubated for 24 h. The next day, the cells were then treated with HCl-48 concentrations ranging 0.3–2.5 µmol/L. After incubation for 24, 48, or 72 h, 20 µL of 3-[4,5-dimethylthiazol-2-yl]-2,5-diphenyltetrazoliumbromide (MTT, Ruitaibio, Chengdu, China) was added and the cells were incubated for 2 h at 37 °C in a 5% CO₂ incubator. The supernatant was then discarded and 100 µL of DMSO (≥99.7%, Sigma–Aldrich) was added to dissolve the formazan crystals. After gentle agitation, the absorbance was measured at 570 nm using the Multiskan GO Microplate Spectrophotometer (Thermo Scientific, Vantaa, Finland).

2.7. Anchorage-independent cell growth

Cells (8 × 10³ cells per well) suspended in complete medium were added to 0.3% agar with 0, 0.3, 0.6 and 1.25 µmol/L HCl-48 in a top layer over a base layer of 0.5% agar containing the same concentration of HCl-48 as the top layer. The cell cultures were

maintained at 37 °C in a 5% CO₂ incubator for 3 weeks and then colonies were randomly selected for imaging using an inverted microscope. The colonies within the representative images were quantified using the Image-Pro Plus software (v.6.1) program (Media Cybernetics, Rockville, MD, USA).

2.8. Cell cycle and apoptosis analyses

The cancer cells (2×10^5 for HCT-15, HCT-116, DLD1 and SW620) were plated in 60 mm plates and treated with HCI-48 (0, 0.3, 0.6 and 1.25 $\mu\text{mol/L}$) for the 48 h. Cells were harvested and fixed in 70%

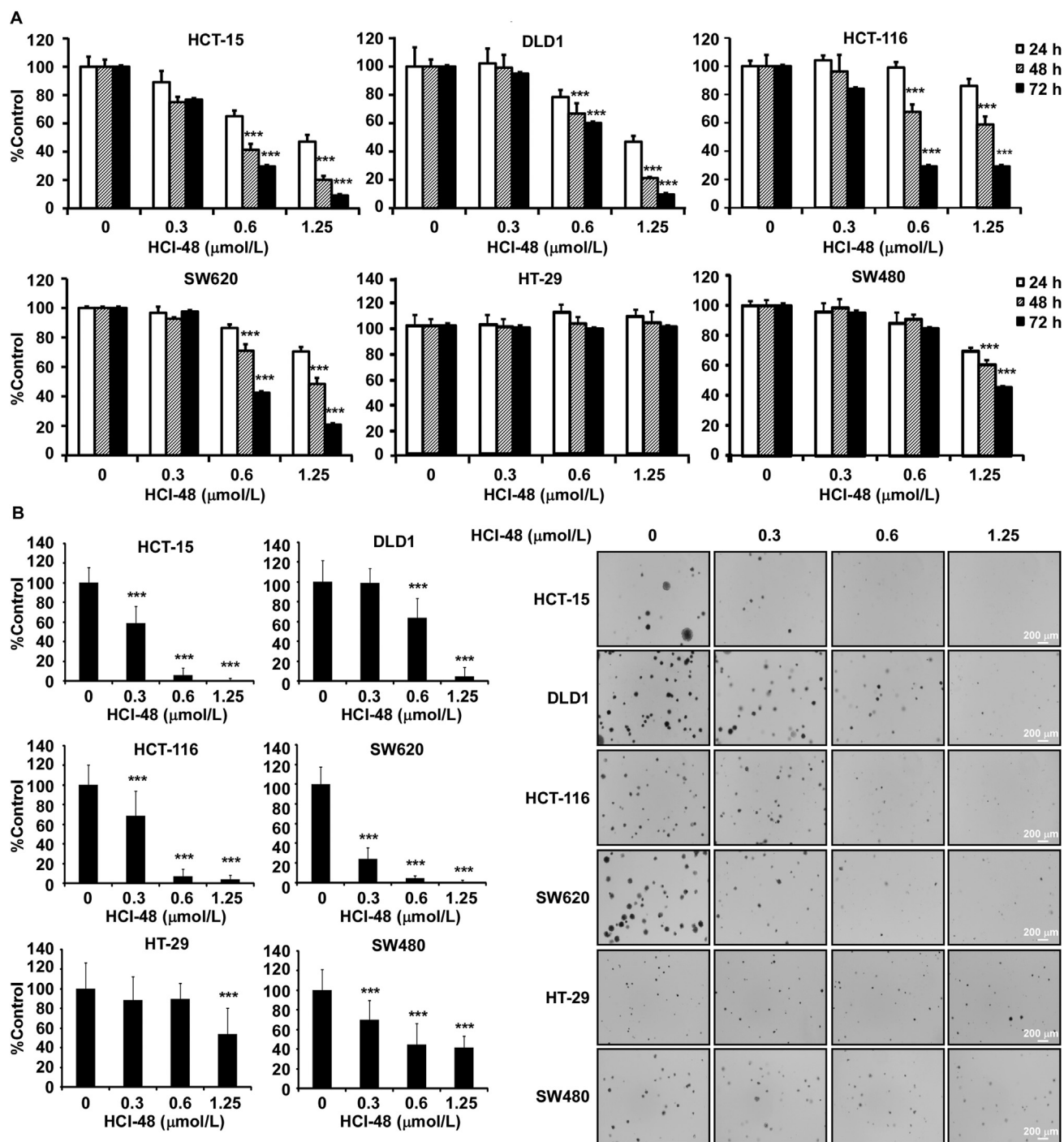


Figure 1 HCI-48 inhibits the proliferation of various colorectal cancer cell lines. (A) The effect of HCI-48 on growth of HCT-15, DLD1, HCT-116, SW620, SW480 and HT-29 cells was estimated by MTT assay at 24, 48, or 72 h ($n = 4$). (B) The effect of HCI-48 on anchorage-independent growth of colon cancer cells was evaluated and representative photographs of the effects of HCI-48 on anchorage-independent growth are shown ($n = 4$). Data are shown as mean \pm SD of values. The asterisks ($*P < 0.05$, $**P < 0.01$, $***P < 0.001$) indicate a significant decrease in proliferation or colony number with HCI-48-treatment compared with untreated control cells.

cold ethanol and stored at -20°C for 24 h. Cells were then stained with $5\ \mu\text{L}$ annexin V and $5\ \mu\text{L}$ $10\ \text{mg/mL}$ propidium iodide for 30 min to check apoptosis or propidium iodide for cell cycle analysis. The cell cycle distribution or apoptosis was determined using FACSscan flow cytometry (BD FACS Calibur flow cytometer, BD Biosciences, San Jose, CA, USA).

2.9. Protein lysate preparation and western blotting

Cells lysates were resolved on ice for 30 min in cell lysis buffer (20 mmol/L Tris, pH 7.5, 150 mmol/L NaCl, 1 mmol/L Na_2EDTA , 1 mmol/L EGTA, 1% Triton X-100, 2.5 mmol/L sodium pyrophosphate, 1 mmol/L β -glycerophosphate, 1 mmol/L sodium vanadate, and 1 mmol/L phenylmethylsulfonyl fluoride). After centrifugation at $18,000 \times g$ (Microfuge 20R, Beckman coulter, CA, USA) for 15 min, the supernatant fractions were harvested as the total cellular protein extracts. The protein concentration was determined using a BCA protein kit (Solarbio life science, Beijing, China) and boiled in $6 \times$ SDS loading buffer. The total

cellular protein extracts were separated by SDS-PAGE and transferred to polyvinylidene fluoride membranes in transfer buffer. Membranes were blocked with 5% non-fat dry milk in $1 \times$ PBST (phosphate buffered saline containing 0.05% Tween-20) and incubated with antibodies against PIM1, p-BAD, BAD, p-FGFR1, FGFR1, p-AKT, AKT, p-STAT3, STAT3, P27, P21, p-histone H3, histone H3, cleaved PARP, PARP, cleaved caspase 3, caspase 3, cleaved caspase 7, caspase 7, cyclin A2 or β -actin in $1 \times$ PBS. Blots were washed 3 times in $1 \times$ PBST buffer, followed by incubation with the appropriate horseradish peroxidase (HRP)-linked IgG. Protein bands were visualized using the enhanced chemiluminescence (ECL) detection reagent (GE Healthcare Life Science, Little Chalfont, HP, UK).

2.10. RNA isolation and quantitative RT-PCR (qRT-PCR) assay

Total RNA was isolated from the tissues of PDX by using TRIzol reagent (Termo Fisher Scientific, Waltham, MA, USA). cDNA was extracted according to the manufacturer's instructions by using the

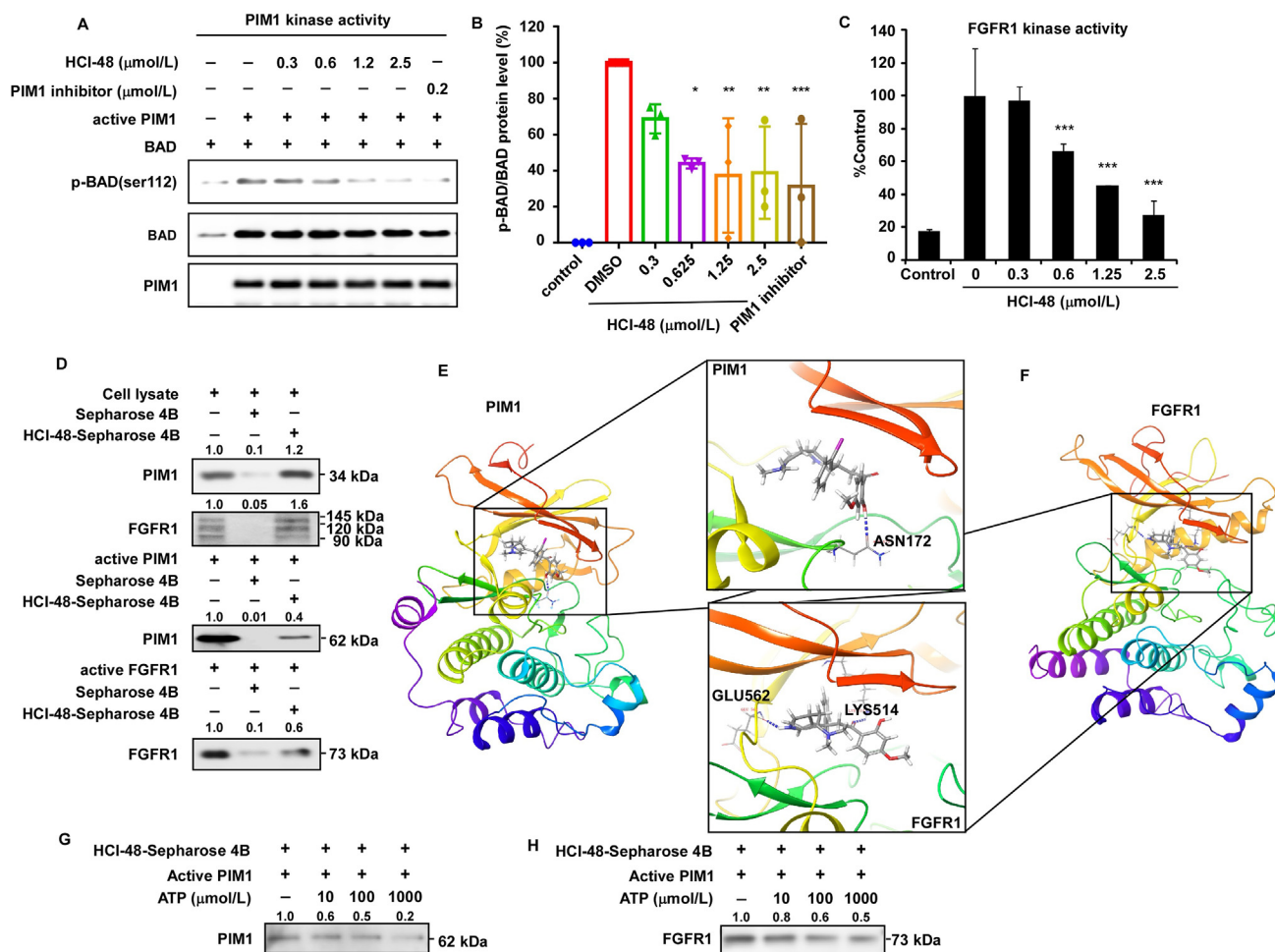


Figure 2 PIM1 and FGFR1 are potential targets of HCl-48. (A) Representative *in vitro* kinase assay analysis of the effect of HCl-48 on PIM1 activity ($n = 3$). (B) Densitometric quantification of three independent experiments. (C) The effect of HCl-48 on FGFR1 activity was evaluated using an *in vitro* kinase assay ($n = 3$). (D) The binding of HCl-48 with PIM1 and FGFR1 in SW620 cell lysate or recombinant PIM1 and FGFR1 were determined using Sepharose 4B and HCl-48-conjugated Sepharose 4B beads ($n = 3$). (E) The interaction between HCl-48 and PIM1 was predicted using a computational docking model. (F) The interaction between HCl-48 and FGFR1 was predicted using a computational docking model. (G, H) The specificity of the binding of HCl-48 on PIM1 or FGFR1 activity was evaluated by ATP concentration ($n = 3$). Data are shown as mean \pm SD of values. For B and C, the asterisks (* $P < 0.05$, ** $P < 0.01$, *** $P < 0.001$) indicate a significant inhibition of PIM1 and FGFR1 kinase activity of HCl-48-treatment compared with untreated control.

RevertAid First Strand cDNA Synthesis Kit (Thermo Fisher Scientific). qRT-PCR was conducted with SYBR Green PCR kit (Takara) on a StepOne Real-Time PCR system (Thermo Fisher Scientific). Relative gene expression levels were determined⁵³. GAPDH was used as the internal control for calculating the relative expression of *Pim1* or *Fgfr1*. The sequences of the primers used are listed in Supporting Information, Table S2.

2.11. In vivo patient-derived xenograft (PDX) mouse model

Six-to eight-week old female NOD.CB17-Prkdcscid/NcrCrl mice (Vital River Labs, Beijing, China) with body weight 18–20 g were used for these experiments. No more than five animals were housed per cage in a specific pathogen-free (SPF) facility using IVC level cages with bedding material made of corncob granules. The mice were maintained on a 12 h/12 h light/dark cycle with food and water available *ad libitum* at $22 \pm 3^\circ\text{C}$ for constant temperature and 40%–70% relative humidity. We studied two cases of colorectal cancer, designated as HJG172 or HJG194, in the PDX animal experiments. HCI-48 was dissolved in 60% DMSO/40% PBS. When tumors reached an average volume of about 100 mm^3 the mice were randomly divided into 3 groups for further experiments as follows:

(1) vehicle group; (2) 1.5 mg/kg of HCI-48; (3) 3 mg/kg of HCI-48. The animal number of each group was ten for the HJG172 models and seven for the HJG194 models. HCI-48 was administered to the mice by intraperitoneal injection once per day for 36 days in the HJG172 model or 64 days in the HJG194 model. Tumor volume was calculated from measurements of the 3 diameters of the individual tumor base using Eq. (1):

$$\text{Tumor volume (mm}^3\text{)} = \text{Length} \times \text{Width} \times \text{Height} \times 0.52 \quad (1)$$

The mice were monitored until the tumors reached a total volume of 1.0 cm^3 . After euthanization with 4% pentobarbital the tumor, liver and spleen from the mice were extracted for further analysis.

2.12. Immunohistochemical (IHC) analysis

After fixation with 4% formaldehyde, tissues were embedded in paraffin blocks, cut and mounted on glass slides. Slides were deparaffinized, hydrated and permeabilized in 300 μL of 0.5% Triton X-100. For immunostaining, tissue slices were then hybridized with Ki-

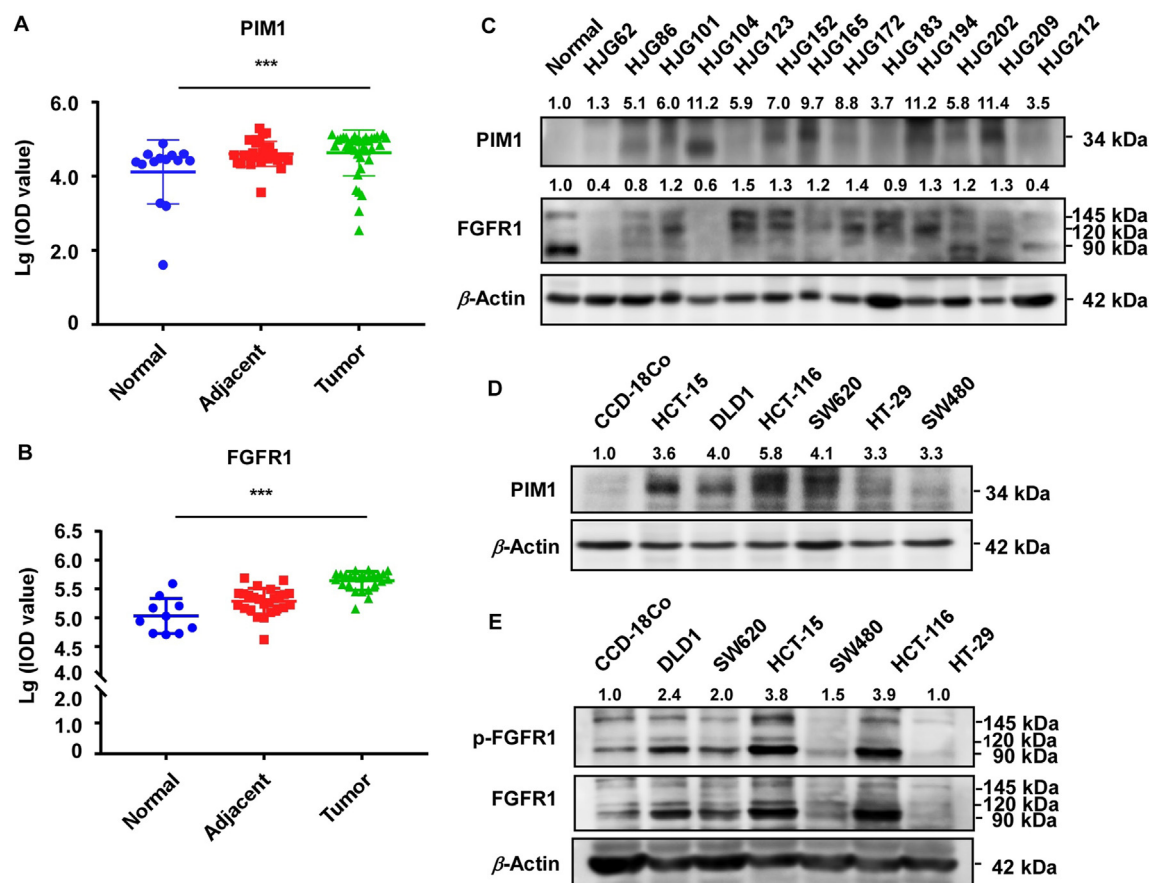


Figure 3 PIM1 and FGFR1 are highly expressed in colorectal cancer. (A) High expression of PIM1 in colorectal patient tissue array: normal ($n = 14$), adjacent ($n = 30$) and tumor ($n = 38$) tissues. (B) High expression of FGFR1 in colorectal patient tissue array: normal ($n = 10$), adjacent ($n = 25$) and tumor ($n = 25$) tissues. (C) The expression of PIM1 and FGFR1 in colorectal cancer tissues ($n = 3$). (D) The expression of PIM1 in colorectal cancer cells and normal cells assessed by western blot analysis ($n = 3$). (E) The expression of FGFR1 in colorectal cancer cells and normal cells assessed by western blot analysis ($n = 3$). Data are shown as mean \pm SD. For A and B, the asterisks (* $P < 0.05$, ** $P < 0.01$, *** $P < 0.001$) indicate significantly elevated expression of PIM1 and FGFR1 in colorectal tissue.

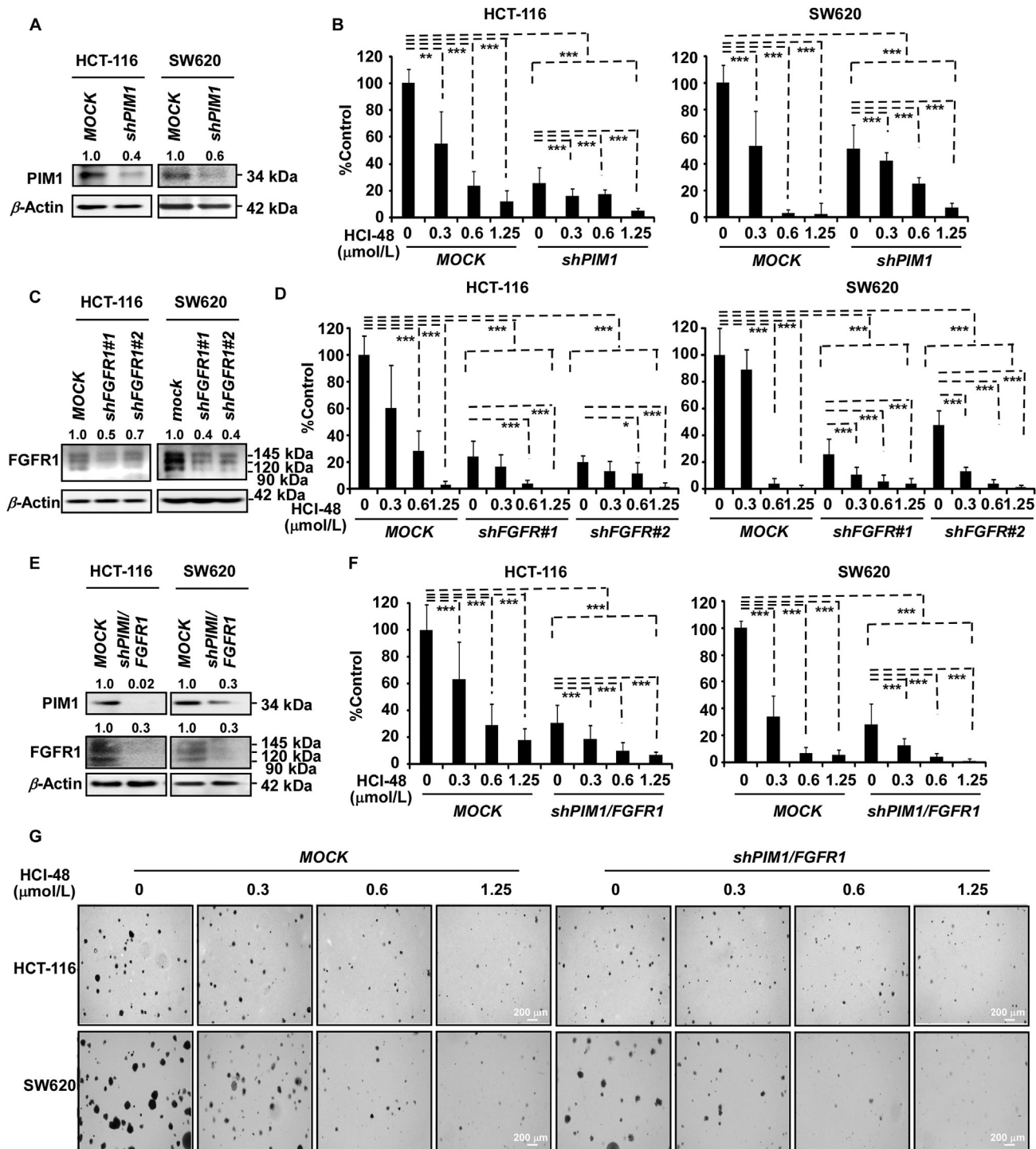


Figure 4 PIM1 and FGFR1 are potential targets in colorectal cancer cells. (A) The expression of PIM1 in HCT-116 and SW620 cells expressing *shMOCK* or *shPIM1* was evaluated by western blotting ($n = 3$). (B) Anchorage-independent cell growth was assessed in HCT-116 and SW620 colorectal cancer cells expressing *shMOCK* or *shPIM1* ($n = 3$). (C) The expression of FGFR1 in HCT-116 and SW620 cells expressing *shMOCK* or *shFGFR1* was evaluated by western blotting ($n = 3$). (D) Anchorage-independent growth was assessed in HCT-116 and SW620 colorectal cancer cells expressing *shMOCK* or *shFGFR1* ($n = 3$). (E) The expression of PIM1 and FGFR1 in HCT-116 and SW620 cells expressing *shMOCK* or *shPIM1/FGFR1* was evaluated by western blotting ($n = 3$). (F) Anchorage-independent growth was assessed in HCT-116 and SW620 colorectal cancer cells expressing *shMOCK* or *shPIM1/FGFR1* ($n = 3$). (G) Representative photographs of the effects of HCl-48 on anchorage-independent growth are shown in HCT-116 and SW620 cells expressing *shMOCK* or *shPIM1/FGFR1* ($n = 3$). Data are shown as mean \pm SD. For B, D, and F, the asterisks ($*P < 0.05$, $**P < 0.01$, $***P < 0.001$) indicate a significant difference in colony formation between *shMOCK* and *shPIM1*, *shFGFR1* or *shPIM1/FGFR1*-expressing cells.

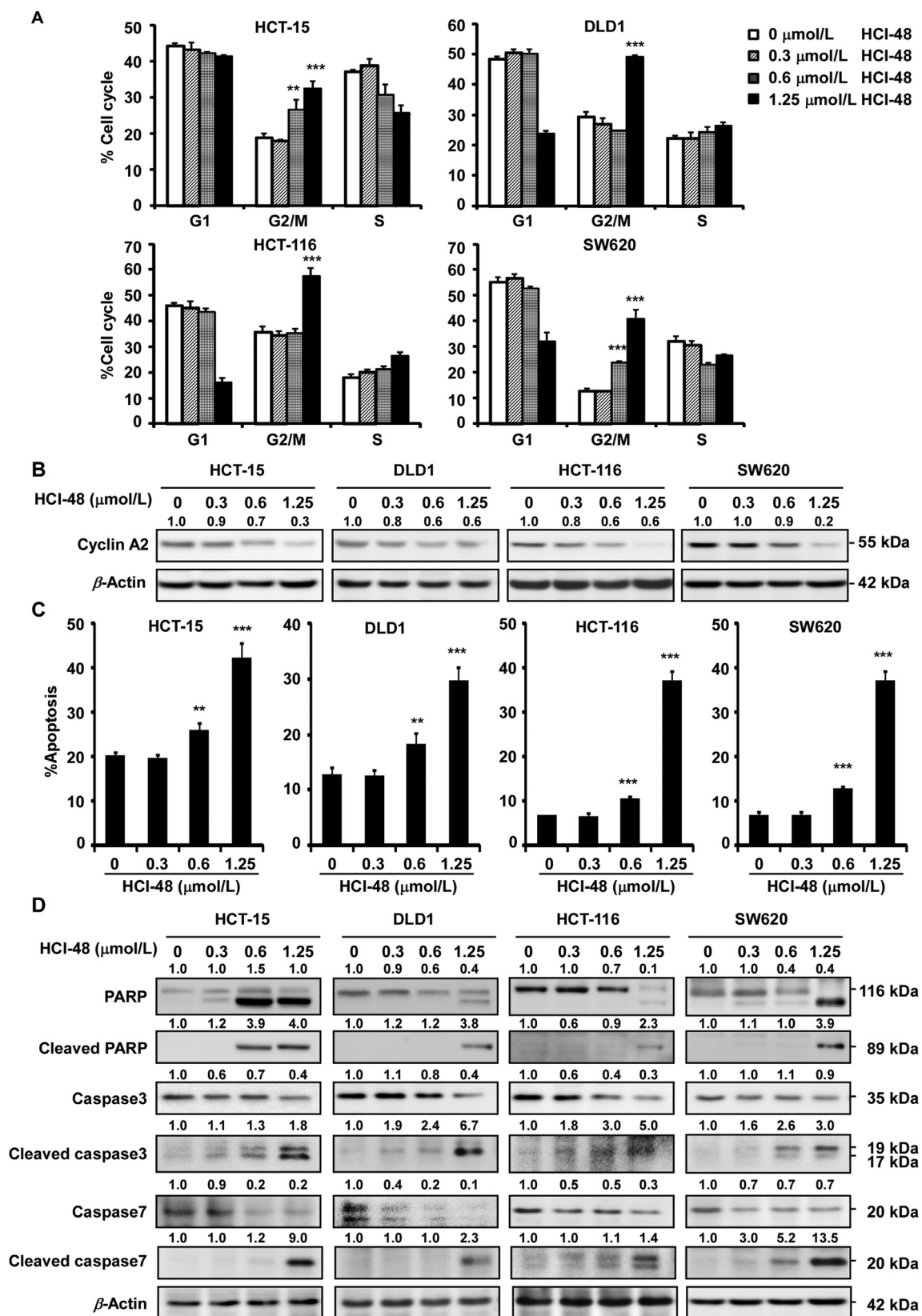


Figure 5 HCI-48 induces cell cycle arrest and apoptosis in colorectal cancer cells. The effects of HCI-48 on cell cycle phase (A) or apoptosis (C) were assessed in colorectal cancer cells. Cells were treated with 0, 0.3, 0.6 or 1.25 $\mu\text{mol/L}$ HCI-48 and then incubated 24 h for cell cycle analysis or for the annexin-V apoptosis assay ($n = 4$). The effects of HCI-48 on the expression of biomarkers associated with cell cycle (B) and apoptosis (D) are shown. Cells were treated with 0, 0.3, 0.6 or 1.25 $\mu\text{mol/L}$ HCI-48 and incubated 24 h for detection of cyclin A2, PARP, cleaved PARP, caspase 3, cleaved caspase 3, caspase 7 and cleaved caspase 7 ($n = 3$). Data are shown as mean \pm SD. The asterisks ($*P < 0.05$, $**P < 0.01$, $***P < 0.001$) indicate a significant difference between untreated control and HCI-48-treated cells.

67 (1:200), p-BAD (1:25), p-FGFR1 (1:100), p-AKT (1:20), p-STAT3 (1:100), PIM1 (1:50), FGFR1 (1:100) or P27 (1:25) as the primary antibody. Biotin-conjugated goat anti-rabbit or mouse IgG was used as the secondary antibody. All sections were randomly imaged by microscope and analyzed using the Image-Pro Plus software (v.6.0) program (Media Cybernetics, Rockville, MD, USA).

2.13. Statistical analysis

The animals were randomized for intervention grouping. Data collection and evaluation of all experiments were performed blind. Quantitative data are expressed as mean \pm standard deviation (SD) and were analyzed using GraphPad Prism v7 (San Diego, California, USA). Statistically significant differences were determined using the Student's *t*-test or one-way ANOVA with Dunn's multiple. A *P* value < 0.05 is considered to be statistically significant. All the *in vitro* experiments were repeated at least three times.

3. Results

3.1. The novel molecule HCI-48 suppresses the proliferation of colorectal cancer cells by targeting PIM1 and FGFR1

As identification of novel efficacious compounds which could treat colon cancer is of utmost importance, we synthesized a panel of drugs based upon the chalcone backbone. From this synthesized panel HCI-48 appeared to be the most effective candidate in inhibiting cell proliferation (Table S1). HCI-48 is modified from the chalcone backbone and the synthesis is shown in Fig. S1A. The novel molecule HCI-48 is $> 95\%$ of purity and the structure was confirmed by NMR analysis (Fig. S1B). To investigate whether HCI-48 inhibits the proliferation of colorectal cancer cells, we first examined the toxicity of HCI-48 on the proliferation of the normal human colon cell line, CCD-18Co (Supporting Information Fig. S2). The results show that HCI-48 didn't affect normal cell

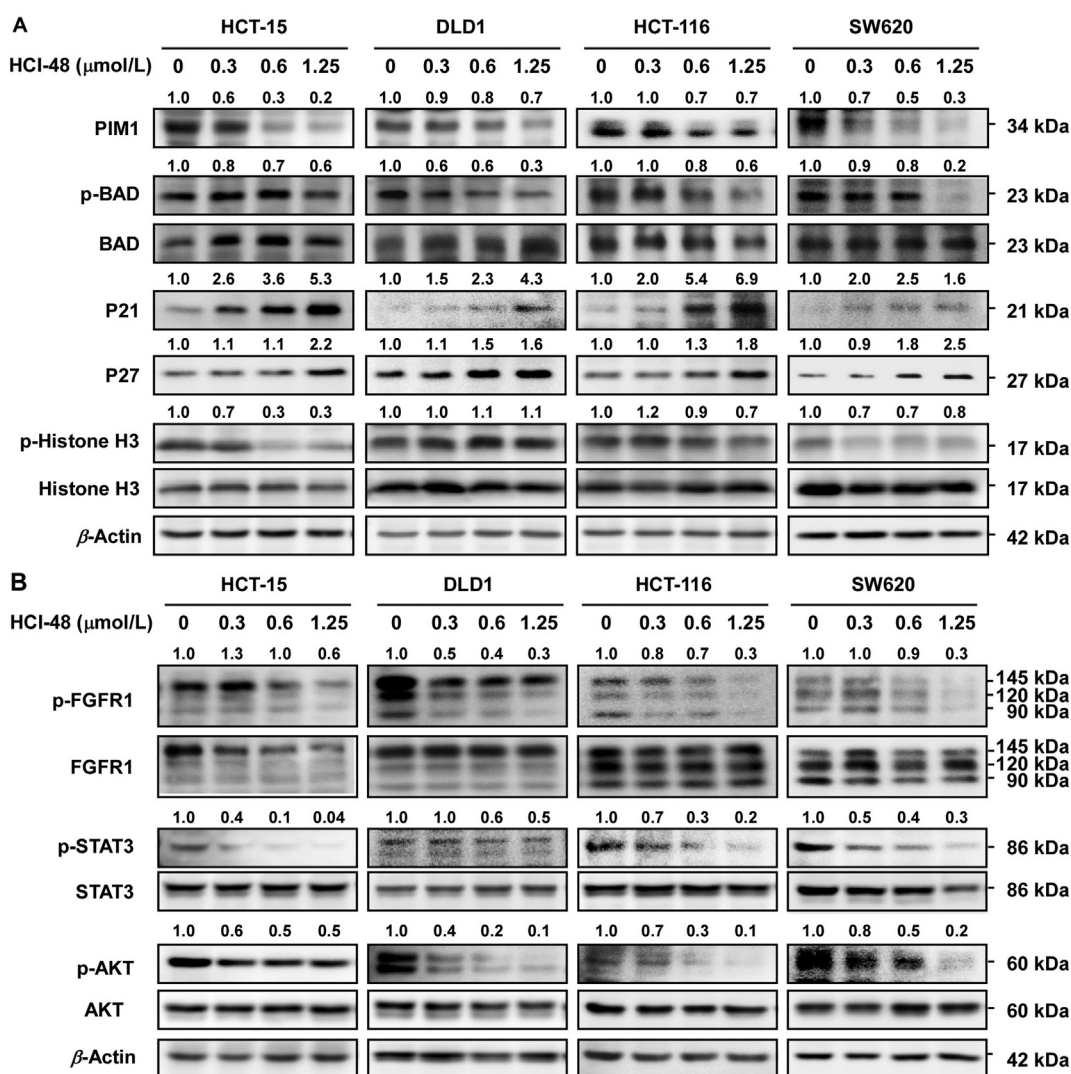


Figure 6 HCI-48 attenuates the expression of proteins involved in PIM1 and FGFR1 signaling. (A) The effect of HCI-48 on PIM1 signaling in colorectal cancer cells was assessed by Western blot analysis. Cells were treated with 0, 0.3, 0.6 or 1.25 $\mu\text{mol/L}$ HCI-48 and harvested at 24 h and then cell lysates were subjected to immunoblotting ($n = 3$). (B) The effect of HCI-48 on FGFR1 signaling in colorectal cancer cells was assessed by Western blot analysis. Cells were treated with 0, 0.3, 0.6 or 1.25 $\mu\text{mol/L}$ HCI-48 and harvested at 24 h and then cell lysates were subjected to western blotting ($n = 3$).

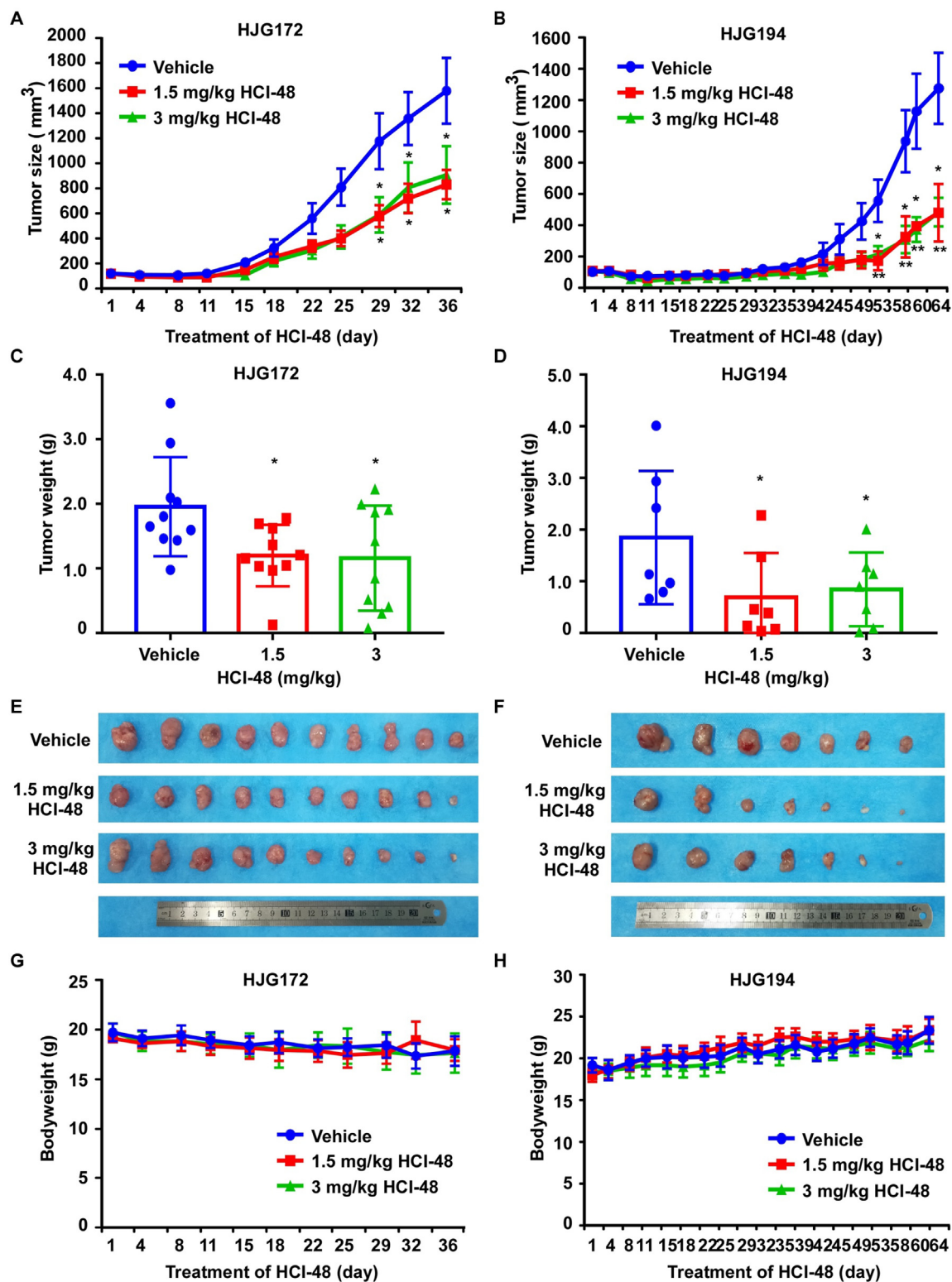


Figure 7 HCI-48 attenuates the growth of patient-derived xenograft tumors in mice (HJG172 and HJG194). (A, B) The effect of HCI-48 on the volume of patient-derived xenograft tumors was plotted 36 days in the case of HJG172 ($n = 10$) and 64 days in the case of HJG194 ($n = 7$) treated with vehicle or HCI-48 (1.5 or 3 mg/kg). For A and B, vehicle or HCI-48 (1.5 or 3 mg/kg) was administered by gavage. Tumor volume was measured twice a week. (C, D) Tumor weight was measured after treatment HCI-48 on the last day of the study. (E, F) Representative photographs of tumor size on the last day of the study. (G, H) No changes in body weight were observed in mice treated with vehicle, 1.5 or 3 mg/kg HCI-48. Data are shown as mean \pm SD. The asterisk ($*P < 0.05$, $**P < 0.01$, $***P < 0.001$) indicates a significant decrease in tumors volume from HCI-48-treated mice compared from vehicle-treated mice.

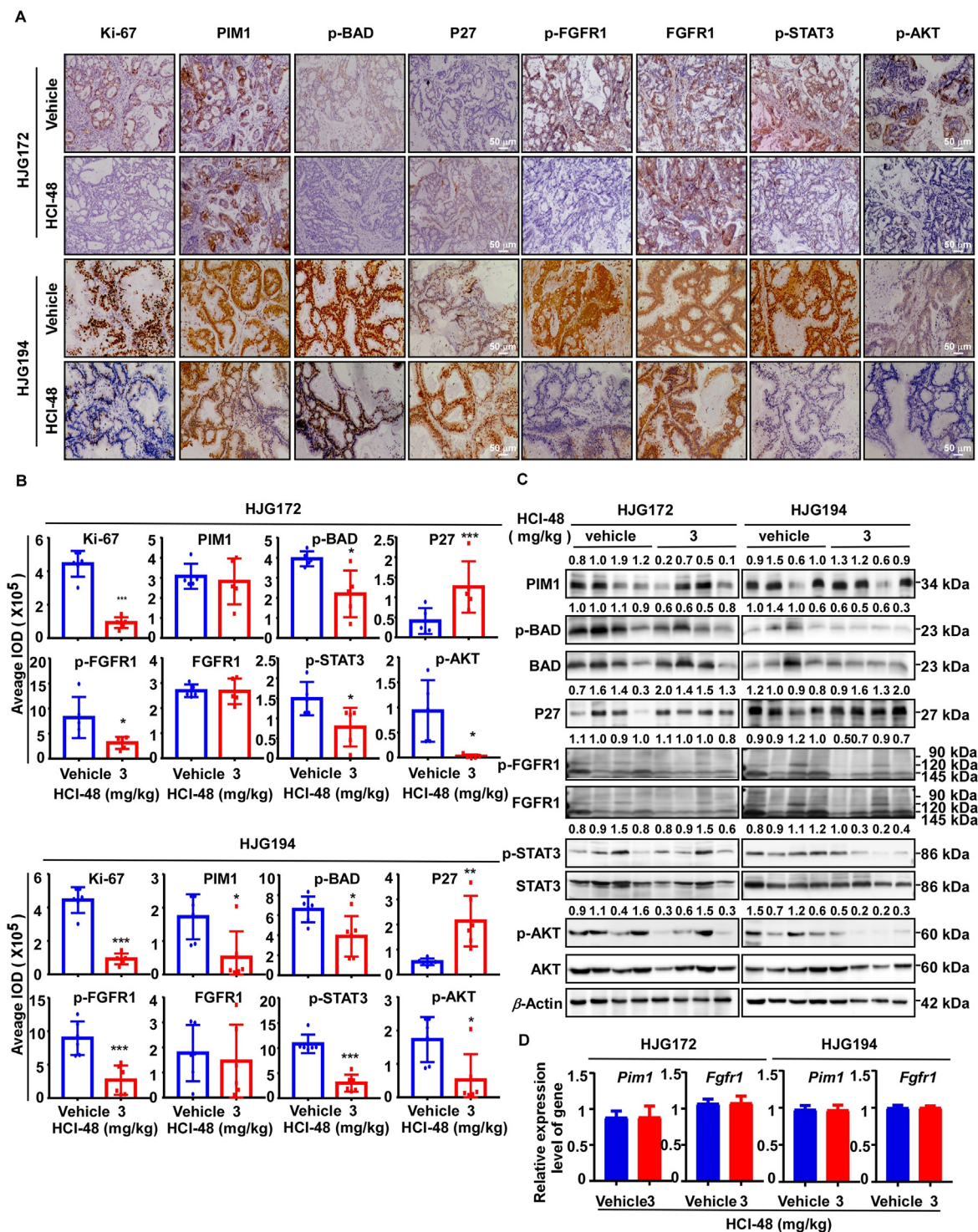


Figure 8 HCl-48 inhibits the expression level of proteins in the PIM1 and FGFR1 signaling pathways in patient-derived xenograft tumor samples. (A) The expression of Ki-67, PIM1, p-BAD, P27, FGFR1, p-FGFR1, p-STAT3 or p-AKT was examined by IHC analysis in patient-derived xenograft tumors of HJG172 ($n = 10$) and HJG194 ($n = 7$). (B) The expression of Ki-67, PIM1, p-BAD, P27, FGFR1, p-FGFR1, p-STAT3 or p-AKT was quantified from 4 separate areas on each slide and an average in HJG172 ($n = 5$) and HJG194 ($n = 6$) in vehicle- and HCl-48-treated groups. (C) The effect of HCl-48 on PIM1 and FGFR1 signaling in patient-derived xenograft tumors of HJG172 and HJG194 assessed by western blot analysis ($n = 4$). (D) The effect of HCl-48 on the gene expression of *Pim1* and *Fgfr1* signaling in patient-derived xenograft tumors of HJG172 and HJG194 was assessed by qRT-PCR analysis ($n = 4$). Data are shown as mean \pm SD. The asterisks (* $P < 0.05$, ** $P < 0.01$, *** $P < 0.001$) indicate a significant decrease in treated tissues compared to untreated controls.

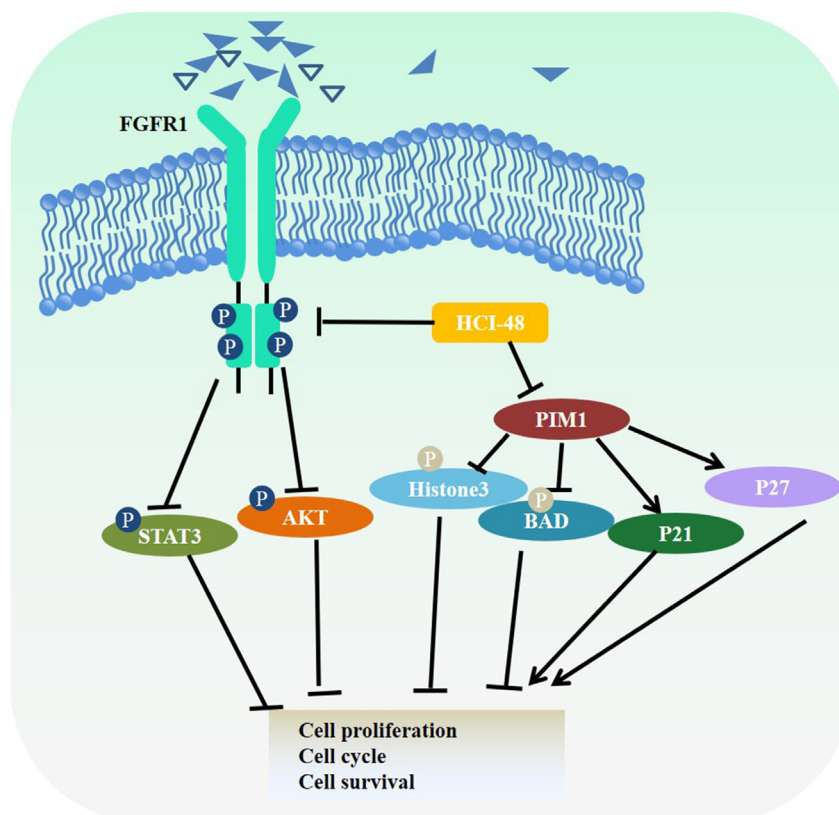


Figure 9 Schematic diagram of the effect of HCI-48 on the FGFR1 and PIM1 signaling pathways.

growth at the highest concentration (2.5 $\mu\text{mol/L}$) and a maximal nontoxic concentration (1.25 $\mu\text{mol/L}$) of HCI-48 was selected for the further experiments. Treatment with HCI-48 (0.3, 0.6, and 1.25 $\mu\text{mol/L}$) strongly suppressed the growth of HCT-15, DLD1, HCT-116 and SW620 colon cancer cells in a time-dependent manner compared to a DMSO control while it showed no significant effect in SW480 and HT-29 cells (Fig. 1A). Using an anchorage-independent cell growth assay, we observed that HCI-48 inhibited the colony number in a concentration-dependent manner compared to a DMSO control. However, this drug showed less effect in SW480 and HT-29 cells (Fig. 1B).

3.2. PIM1 and FGFR1 are targets of HCI-48

In order to study the inhibitory mechanism of HCI-48, we performed a kinase profiling assay in the presence of HCI-48 at 20 $\mu\text{mol/L}$ against a panel of roughly 100 kinases. The data show that the activities of FGFR1 and PIM1 were inhibited by 34% and 56%, respectively, with a lesser inhibitory effect on other kinases (Supporting Information Table S3). This suggested that the major targets of HCI-48 are PIM1 and FGFR1. Next, we performed an *in vitro* kinase assay to confirm the effect of HCI-48 and observed that HCI-48 significantly inhibited the kinase activity of both PIM1 (Fig. 2A and B) and FGFR1 (Fig. 2C). The IC_{50} values of HCI-48 for inhibition of PIM1 and FGFR1 were 0.5 and 1.1 $\mu\text{mol/L}$, respectively. Based on these results, we assessed drug binding and interaction by an *ex vivo* or *in vitro* binding assay. HCI-48 bound to recombinant active PIM1 and FGFR1 as well as PIM1 and FGFR1 in cell lysates (Fig. 2D). Additionally, we utilized a computational docking model to validate the potential interaction between HCI-48 and PIM1 or FGFR1 (Fig. 2E and F).

According to the computer docking model, HCI-48 can interact with asparagine (ASN) 172, and lysine (LYS) 514 and glutamic acid (GLU) 562 sites of the PIM1 and FGFR1 active pockets (Fig. 2E and F). The binding of HCI-48 with PIM1 and FGFR1 in the presence of ATP (10, 100, or 1000 $\mu\text{mol/L}$) was reduced as ATP concentration was increased (Fig. 2G and H), indicating that HCI-48 interacts with the ATP-binding pocket of PIM1 and FGFR1. These results indicate that HCI-48 could be a therapeutically effective inhibitor of PIM1 and FGFR1 and can directly inhibit both PIM1 and FGFR1 kinase activities in an ATP-dependent manner.

3.3. PIM1 and FGFR1 are potential targets of HCI-48 in colorectal cancer

To determine the expression level of FGFR1 and PIM1 in colorectal cancer, we performed an immunohistochemical analysis and western blot assay (Fig. 3A–E). The results indicate that PIM1 and FGFR1 are highly expression in colorectal patient tissues and patient-derived xenograft samples as compared to normal or adjacent tissues (Fig. 3A–C). Moreover, the sensitive cell lines (HCT-15, DLD1, HCT-116 and SW620) showed higher expression of PIM1 and FGFR1 than the less sensitive HT-29 and SW480 cell lines (Fig. 3D–E).

To verify whether PIM1 and FGFR1 are plausible molecular targets for the anti-proliferative activity of HCI-48, we prepared PIM1 and FGFR1 knock-down cells by infecting cells with virus particles containing *shMOCK*, *shPIM1* or *shFGFR1* (Fig. 4A, C and E) and then conducted an anchorage-independent cell growth assay (Fig. 4B, D and F). Western blot results verified the knockdown of PIM1 or FGFR1 expression in HCT-116 and SW620 cells (Fig. 4A, C and E). The colony number of cells

infected with *shPIM1* or *shFGFR1* was decreased in both knockdown cell lines. Additionally, the anti-proliferative effect of HCI-48 on the tested cells was decreased compared to *shMOCK* transfected cells (Fig. 4B and D). Thus, combination silencing of PIM1 and FGFR1 expression in colorectal cells decreased the colony numbers and showed less sensitivity to HCI-48 treatment compared to *shMOCK* transfected cells (Fig. 4F and G).

3.4. HCI-48 induces cell cycle at G2 phase and apoptosis of colon cancer cell lines

To further confirm the anticancer potential of HCI-48, we used flow cytometry to examine whether the inhibition PIM1 and FGFR1 activities and expression could contribute to cell cycle arrest and apoptosis. Treatment with HCI-48 induced the G2/M phase arrest in HCT-15, DLD1, HCT-116 and SW620 cells (Fig. 5A). Based on the cell cycle analysis results, we examined the expression of cyclin A2, a marker associated with the G2/M phase, in HCI-48-treated cells using western blotting. We observed that HCI-48 reduced the expression of cyclin A2 in HCT-15, DLD1, HCT-116 and SW620 cancer cells compared with the DMSO-treated control (Fig. 5B). Treatment with HCI-48 also induced apoptosis in colon cancer cells as evidenced by flow cytometry results (Fig. 5C). Therefore, we measured apoptosis markers using western blotting. The results show that HCI-48 treatment increased the expression of cleaved PARP, cleaved caspase 3 and cleaved caspase 7 and decreased the expression of intact PARP, caspase 3 and caspase 7 in HCT-15, DLD1, HCT-116 and SW620 cells (Fig. 5D).

3.5. HCI-48 inhibits PIM1 and FGFR1 signaling pathways

Given the ability of HCI-48 to inhibit growth and induce apoptosis in colon cancer cells by targeting PIM1 and FGFR1, we determined the effect of HCI-48 on the expression of PIM1 and FGFR1 and their down-stream signaling cascades.

HCT-15, DLD1, HCT-116 and SW620 cells were treated with HCI-48 for 24 h and cell lysates were prepared. We observed that the expression of PIM1, p-BAD, P21, P27, p-Histone H3, p-FGFR1, p-AKT and p-STAT3, proteins belonging to the PIM1 and FGFR1 signaling pathways were suppressed in a dose-dependent manner. However, total protein levels of PIM1, FGFR1, BAD, Histone H3, AKT and STAT3 did not significantly change (Fig. 6A and B).

3.6. HCI-48 inhibits tumor growth of patient-derived xenografts

To provide evidence that HCI-48 can suppress colon cancer cell growth *in vivo*, we studied the effect of HCI-48 on two PDX models designated as HJG172 and HJG194. The PDX tumor samples were obtained from patients who had undergone surgical resection and show high expression of PIM1 and FGFR1 (Supporting Information Fig. S3A). The PDX tumors were implanted into mice and then treated with vehicle or HCI-48 (1.5 or 3 mg/kg) *via* intraperitoneal injection once per day for 36 or 64 days. The results show that the treatment of mice with 1.5 and 3 mg/kg of HCI-48 significantly reduced the tumor growth of both cases compared to a vehicle-treated group (Fig. 7A–F) with no effect on body, spleen or liver weight (Figs. 7G and H, S3B and S3C).

To evaluate these results, we measured Ki-67 and the target signaling pathway proteins in tissue samples derived from HCI-

48-treated mice (Fig. 8A and B). IHC analysis indicated that HCI-48 suppressed the expression of the Ki-67 proliferation marker in both the HJG172 and HJG194 cases compared to tissue derived from vehicle-treated mice. Moreover, HCI-48 down-regulated PIM1, p-BAD, and p-FGFR1, p-STAT3 and p-AKT while up-regulating P27 expression compared with vehicle-treated controls and measured by IHC and Western blot analysis. No changes in FGFR1, STAT3 and AKT protein expression were observed (Fig. 8A–C), and there was no change in the expression of *Pim1* and *Fgfr1* (Fig. 8D).

4. Discussion

Chalcone inhibits the growth of breast cancer cells by regulating the cell cycle and apoptosis⁵⁴. A previous study discovered novel chalcone derivatives as potential inhibitors of epidermal growth factor receptor (EGFR) for treatment of bladder cancer⁵⁵. Khan et al.⁵⁶ similarly studied the application of pyrazole chalcone compounds as EGFR/AKT pathway inhibitors in cancer. Additionally, Gil et al.⁵⁷ have designed and synthesized a synthetic trimethoxy chalcone derivative to study the effect on P53 in A549 lung cancer cells. To find a promising therapeutic compound for CRC, we synthesized many chalcone derivatives. We measured the activity of many indoles using an MTT assay and identified the most effective small molecule compound, HCI-48, based on its IC₅₀ (Table S1). HCI-48 is an indole derivative of chalcone, which has documented anti-tumor effects. Studies demonstrated that indole-chalcone could inhibit multidrug-resistant cancer cell growth by targeting microtubules⁵⁸. However, the target of indole-chalcone in colorectal cancer has not been reported, and the mechanisms underlying potential chemopreventive effects remain unresolved. Thus, the focus of this study was to identify the target of HCI-48, with kinase profiling analysis showing that HCI-48 strongly inhibited the kinase activity of PIM1 and FGFR1. These results suggested that kinases PIM1 and FGFR1 may be major targets of HCI-48. We further explored the molecular mechanism of HCI-48 as an inhibitor of PIM1 and FGFR1 kinases in colorectal cancer cells.

The results of *in vitro* kinase assays showed that HCI-48 significantly inhibited PIM1 and FGFR1 kinase activities (Fig. 2). BAD protein is a pro-apoptotic protein involved in the initiation of apoptosis in the BCL-2 gene family, and PIM1 phosphorylates BAD at Ser112, thus promoting cell proliferation and apoptosis⁵⁹. Zippo et al.⁶⁰ showed that histone H3 is a substrate of PIM1 with the down-regulation of p-histone H3 (Ser10). When FGF binds to FGFR1, FGFR1 can alter cell proliferation, differentiation, and migration by activating the AKT and STAT signaling pathways⁶¹. Our study shows that as the concentration of HCI-48 increased, phosphorylation levels of BAD decreased. Additionally, the activity of FGFR1 is also decreased, suggesting that HCI-48 can target PIM1 and FGFR1, and then inhibit their activity by competitively binding with ATP in a docking model assay (Fig. 2). High expression levels of PIM1 can promote the proliferation of colorectal cancer cells. Therefore, HCI-48 targeting PIM1 and FGFR1 simultaneously may be a good strategy for the treatment of colorectal cancer. Western blotting results showed that PIM1 and FGFR1 were highly expressed in the colorectal cancer cell lines HCT-15, DLD1, HCT-116 and SW620 (Fig. 3). MTT and soft agar assays showed that HCI-48 had no cytotoxicity at 2.5 μmol/L and significantly inhibited the proliferation of colorectal cancer cells, especially in cells with high expression of PIM1 and FGFR1 (HCT-15, DLD1, HCT-116, and SW620) (Figs. 1 and 3). We next simultaneously knocked down

expression of PIM1 and FGFR1 to determine if the activity of HCI-48 is dependent upon the presence of these two kinases. A soft agar assay showed that the anti-tumor effect of HCI-48 on CRC cells with reduced PIM1 and FGFR1 was significantly reduced (Fig. 4). Hu et al.⁶² showed that the activity of cyclin A2 begins in early S phase, increases in the G2/M phase, and plays an important role in regulating the entry to mitosis. Western blotting results with HCI-48-treated cells showed that the expression of cyclin A2, a protein marker in the G2/M phase, decreased. Nava-Tapia et al.⁶³ showed that brazilin inhibits cell proliferation and induces apoptosis through increased expression of P21, P27, activation of caspase 3 and caspase 7, and the cleaved PARP. Our immunoblotting results with HCI-48-treated cells showed that the expression of PARP, caspase 3 and caspase 7, the key executors of cell apoptosis, was decreased. Flow cytometry analysis also confirmed that HCI-48 could arrest the cell cycle at the G2/M phase and induce cell apoptosis (Fig. 5). PIM1 kinase plays a key role in cell cycle regulation, phosphorylates its substrate BAD, activates downstream signaling pathways, affects P21 and P27, and regulates the cell cycle. Additionally, activation of FGFR1 targets STAT and AKT signaling pathways, further affecting cell proliferation⁶⁴, and our study shows that HCI-48 inhibits the activity of both FGFR1 and PIM1 signaling pathways (Fig. 6).

The role of the PDX model in preclinical studies is to identify therapeutic targets, including specific molecules and molecular interactions, and to serve as a guide for clinical treatment of cancer⁶⁵. Therefore, chemoprophylaxis with HCI-48 in a PDX model is an important part of this study. Two xenograft models, HJG172 and HJG194, derived from colorectal tissues expressing high levels PIM1 and FGFR1, were selected for testing. HCI-48 exhibited no toxic effect as evidenced by maintenance of body weight, liver weight and spleen weight (Fig. S3). Most importantly, tumor volume and weight decreased upon treatment, suggesting that HCI-48 can inhibit the proliferation of colorectal cancer *in vivo* (Fig. 7).

We analyzed the xenograft tumors *via* IHC and WB analysis. The results indicate that HCI-48 down-regulated Ki-67, PIM1, p-BAD, and p-FGFR1, p-STAT3 and p-AKT and promoted P27 expression in the PDX models. Additionally, quantitative RT-PCR analysis showed that the gene expression level of *Pim1* and *Fgfr1* did not change in the HCI-48-treated group (Fig. 8). Together, these results indicate the potential of developing HCI-48 as a novel inhibitor of PIM1 and FGFR1 for CRC.

5. Conclusions

This study demonstrates that the new small-molecule synthetic compound HCI-48 inhibits PIM1 and FGFR1 activity directly and attenuates their downstream signaling pathways, thus indicating that HCI-48 can inhibit the proliferation of colorectal cancer *in vivo* and *in vitro* (Fig. 9); we believe the therapeutic potential of HCI-48 in the treatment of colorectal cancer warrants further study.

Acknowledgments

This work was supported by grant funding from the National Natural Science Foundation of China (81972839, 82002620 and 82073075), and the Scientific and Technological Project in Henan Province and Henan Provincial Government (Nos. 212102310882, and 222102310104, China). We wish to thank Dr. Xiang Li, Ran Yang, Sen Yang, and Fangfang Liu in the China-US (Henan) Hormel Cancer Institute, Zhengzhou, China for supporting materials and

experiments, and Dr. Jaeki Min in Induced Proximity Platform (IPP) Amgen, USA for discussing the HCI-48 compound.

Author contributions

Fanxiang Yin, Ran Zhao, Mee-Hyun Lee and Zigang Dong are involved in study concept and design, acquisition of data, analysis and interpretation of data, drafting of the manuscript. Fanxiang Yin, Ran Zhao, Hanyong Chen, Xiaorong Fu, Ning Lu, Hai Huang, and Beibei Xu performed experiments. Zigang Dong, Dhilli Rao Gorja, Jung-Hyun Shim, Zhi Li and Kangdong Liu provided material support. Fanxiang Yin, Ran Zhao, Mee-Hyun Lee, Kangdong Liu, Kyle Vaughn Laster and Zigang Dong wrote the manuscript. Zigang Dong and Mee-Hyun Lee had supervision of all study. All authors read and approved the final manuscript.

Conflicts of interest

The authors declare no conflicts of interest.

Appendix A. Supporting information

Supporting information to this article can be found online at <https://doi.org/10.1016/j.apsb.2022.07.005>.

References

1. Siegel RL, Miller KD, Fuchs HE, Jemal A. Cancer statistics, 2021. *CA Cancer J Clin* 2021;**71**:7–33.
2. Zhou J, Zheng R, Zhang S, Zeng H, Wang S, Chen R, et al. Colorectal cancer burden and trends: comparison between China and major burden countries in the world. *Chin J Cancer Res* 2021;**33**:1–10.
3. Winkels RM, Kampman E, Wu M. Learning from East to West and *vice versa*: clinical epidemiology of colorectal cancer in China. *Cancer* 2021;**127**:1736–8.
4. Yang T, Li X, Montazeri Z, Little J, Farrington SM, Ioannidis JPA, et al. Gene-environment interactions and colorectal cancer risk: an umbrella review of systematic reviews and meta-analyses of observational studies. *Int J Cancer* 2019;**145**:2315–29.
5. Bray C, Bell LN, Liang H, Collins D, Yale SH. Colorectal cancer screening. *Wis Med J* 2017;**116**:27–33.
6. Solomon BL, Whitman T, Wood ME. Contribution of extended family history in assessment of risk for breast and colon cancer. *BMC Fam Pract* 2016;**17**:126.
7. El Kinany K, Huybrechts I, Kampman E, Boudouaya HA, Hatime Z, Mint Sidi Deoula M, et al. Concordance with the World Cancer Research Fund/American Institute for cancer research recommendations for cancer prevention and colorectal cancer risk in Morocco: a large, population-based case-control study. *Int J Cancer* 2019;**145**:1829–37.
8. Thanikachalam K, Khan G. Colorectal cancer and nutrition. *Nutrients* 2019;**11**:164.
9. Shahjehan F, Merchea A, Cochuyt JJ, Li Z, Colibaseanu DT, Kasi PM. Body mass index and long-term outcomes in patients with colorectal cancer. *Front Oncol* 2018;**8**:620.
10. Barnung RB, Jareid M, Lukic M, Oyeyemi SO, Rudolfson JH, Sovershaeva E, et al. High lactose whey cheese consumption and risk of colorectal cancer—the Norwegian Women and Cancer Study. *Sci Rep* 2019;**9**:296.
11. Ma Y, Yang Y, Wang F, Zhang P, Shi C, Zou Y, et al. Obesity and risk of colorectal cancer: a systematic review of prospective studies. *PLoS One* 2013;**8**:e53916.
12. Fagunwa IO, Loughrey MB, Coleman HG. Alcohol, smoking and the risk of premalignant and malignant colorectal neoplasms. *Best Pract Res Clin Gastroenterol* 2017;**31**:561–8.

13. Yahagi M, Tsuruta M, Hasegawa H, Okabayashi K, Toyoda N, Iwama N, et al. Smoking is a risk factor for pulmonary metastasis in colorectal cancer. *Colorectal Dis* 2017;**19**:O322–8.
14. Rangu V, Sund ER, Mork PJ, Roe OD, Bauman A. The associations of sitting time and physical activity on total and site-specific cancer incidence: results from the HUNT study, Norway. *PLoS One* 2018;**13**: e0206015.
15. Watson AJ, Collins PD. Colon cancer: a civilization disorder. *Dig Dis* 2011;**29**:222–8.
16. Liu K, Gao H, Wang Q, Wang L, Zhang B, Han Z. Hispidulin suppresses cell growth and metastasis by targeting PIM1 through JAK2/STAT3 signaling in colorectal cancer. *Cancer Sci* 2018;**109**: 1369–81.
17. Maida M, Macaluso FS, Ianiro G, Mangiola F, Sinagra E, Hold G, et al. Screening of colorectal cancer: present and future. *Expert Rev Anticancer Ther* 2017;**17**:1131–46.
18. Roessler S, Jia HL, Budhu A, Forgues M, Ye QH, Lee JS, et al. A unique metastasis gene signature enables prediction of tumor relapse in early-stage hepatocellular carcinoma patients. *Cancer Res* 2010;**70**: 10202–12.
19. Yu X, Zheng B, Chai R. Lentivirus-mediated knockdown of eukaryotic translation initiation factor 3 subunit D inhibits proliferation of HCT116 colon cancer cells. *Biosci Rep* 2014;**34**:e00161.
20. Ciombor KK, Wu C, Goldberg RM. Recent therapeutic advances in the treatment of colorectal cancer. *Annu Rev Med* 2015;**66**:83–95.
21. Golob-Schwarzl N, Schweiger C, Koller C, Krassnig S, Gogg-Kamerer M, Gantenbein N, et al. Separation of low and high grade colon and rectum carcinoma by eukaryotic translation initiation factors 1, 5 and 6. *Oncotarget* 2017;**8**:101224–43.
22. Li Z, Lin F, Zhuo C, Deng G, Chen Z, Yin S, et al. PIM1 kinase phosphorylates the human transcription factor FOXP3 at serine 422 to negatively regulate its activity under inflammation. *J Biol Chem* 2014;**289**:26872–81.
23. Peng YH, Li JJ, Xie FW, Chen JF, Yu YH, Ouyang XN, et al. Expression of pim-1 in tumors, tumor stroma and tumor-adjacent mucosa co-determines the prognosis of colon cancer patients. *PLoS One* 2013;**8**:e76693.
24. Kim J, Roh M, Abdulkadir SA. Pim1 promotes human prostate cancer cell tumorigenicity and c-MYC transcriptional activity. *BMC Cancer* 2010;**10**:248.
25. Zhang X, Song M, Kundu JK, Lee MH, Liu ZZ. PIM kinase as an executional target in cancer. *J Cancer Prev* 2018;**23**:109–16.
26. Herzog S, Fink MA, Weitmann K, Friedel C, Hadlich S, Langner S, et al. Pim1 kinase is upregulated in glioblastoma multiforme and mediates tumor cell survival. *Neuro Oncol* 2015;**17**:223–42.
27. Leung CO, Wong CC, Fan DN, Kai AK, Tung EK, Xu IM, et al. PIM1 regulates glycolysis and promotes tumor progression in hepatocellular carcinoma. *Oncotarget* 2015;**6**:10880–92.
28. Amaravadi R, Thompson CB. The survival kinases Akt and Pim as potential pharmacological targets. *J Clin Invest* 2005;**115**:2618–24.
29. Xian W, Schwertfeger KL, Vargo-Gogola T, Rosen JM. Pleiotropic effects of FGFR1 on cell proliferation, survival, and migration in a 3D mammary epithelial cell model. *J Cell Biol* 2005;**171**: 663–73.
30. Weiss J, Sos ML, Seidel D, Peifer M, Zander T, Heuckmann JM, et al. Frequent and focal FGFR1 amplification associates with therapeutically tractable FGFR1 dependency in squamous cell lung cancer. *Sci Transl Med* 2010;**2**:62ra93.
31. Tomlinson DC, Lamont FR, Shnyder SD, Knowles MA. Fibroblast growth factor receptor 1 promotes proliferation and survival via activation of the mitogen-activated protein kinase pathway in bladder cancer. *Cancer Res* 2009;**69**:4613–20.
32. Futami T, Okada H, Kihara R, Kawase T, Nakayama A, Suzuki T, et al. ASP5878, a novel inhibitor of FGFR1, 2, 3, and 4, inhibits the growth of FGF19-expressing hepatocellular carcinoma. *Mol Cancer Ther* 2017;**16**:68–75.
33. Preusser M, Berghoff AS, Berger W, Ilhan-Mutlu A, Dinhof C, Widhalm G, et al. High rate of FGFR1 amplifications in brain metastases of squamous and non-squamous lung cancer. *Lung Cancer* 2014;**83**:83–9.
34. Gao G, Tian Z, Zhu HY, Ouyang XY. miRNA-133b targets FGFR1 and presents multiple tumor suppressor activities in osteosarcoma. *Cancer Cell Int* 2018;**18**:210.
35. De Luca A, Frezzetti D, Gallo M, Normanno N. FGFR-targeted therapeutics for the treatment of breast cancer. *Expert Opin Investig Drugs* 2017;**26**:303–11.
36. Perez-Garcia J, Munoz-Couselo E, Soberino J, Racca F, Cortes J. Targeting FGFR pathway in breast cancer. *Breast* 2018;**37**:126–33.
37. Orlikova B, Tasdemir D, Golais F, Dicato M, Diederich M. Dietary chalcones with chemopreventive and chemotherapeutic potential. *Genes Nutr* 2011;**6**:125–47.
38. Cao Y, Xu Wenxing, Huang Yiyu, Xing Z, Licochalcone B. A chalcone derivative from *Glycyrrhiza inflata*, as a multifunctional agent for the treatment of Alzheimer's disease. *Nat Prod Res* 2020;**34**: 736–9.
39. Srinivasan B, Johnson TE, Lad R, Xing C. Structure–activity relationship studies of chalcone leading to 3-hydroxy-4,3',4',5'-tetramethoxychalcone and its analogues as potent nuclear factor kappaB inhibitors and their anticancer activities. *J Med Chem* 2009;**52**: 7228–35.
40. Modzelewska A, Pettit C, Achanta G, Davidson NE, Huang P, Khan SR. Anticancer activities of novel chalcone and bis-chalcone derivatives. *Bioorg Med Chem* 2006;**14**:3491–5.
41. Wu J, Li J, Cai Y, Pan Y, Ye F, Zhang Y, et al. Evaluation and discovery of novel synthetic chalcone derivatives as anti-inflammatory agents. *J Med Chem* 2011;**54**:8110–23.
42. Maria K, Dimitra HL, Maria G. Synthesis and anti-inflammatory activity of chalcones and related Mannich bases. *Med Chem* 2008;**4**: 586–96.
43. Ayman M, El-Messery SM, Habib EE, Al-Rashood ST, Almethizia AA, Alkahtani HM, et al. Targeting microbial resistance: synthesis, antibacterial evaluation, DNA binding and modeling study of new chalcone-based dithiocarbamate derivatives. *Bioorg Chem* 2019;**85**:282–92.
44. Mathaiyan M, Suresh A, Balamurugan R. Binding property of HIV p24 and reverse transcriptase by chalcones from *Pongamia pinnata* seeds. *Bioinformation* 2018;**14**:279–84.
45. Sakata RP, Figueiro M, Kawano DF, Almeida WP. Effect on acetylcholinesterase and anti-oxidant activity of synthetic chalcones having a good predicted pharmacokinetic profile. *Med Chem* 2017;**13**: 654–63.
46. Iwamura C, Shinoda K, Yoshimura M, Watanabe Y, Obata A, Nakayama T. Naringenin chalcone suppresses allergic asthma by inhibiting the type-2 function of CD4 T cells. *Allergol Int* 2010;**59**: 67–73.
47. Robinson MW, Overmeyer JH, Young AM, Erhardt PW, Maltese WA. Synthesis and evaluation of indole-based chalcones as inducers of methuosis, a novel type of nonapoptotic cell death. *J Med Chem* 2012;**55**:1940–56.
48. Oh HN, Lee MH, Kim E, Yoon G, Chae JI, Shim JH. Licochalcone B inhibits growth and induces apoptosis of human non-small-cell lung cancer cells by dual targeting of EGFR and MET. *Phytomedicine* 2019;**63**:153014.
49. Hsu YL, Kuo PL, Tzeng WS, Lin CC. Chalcone inhibits the proliferation of human breast cancer cell by blocking cell cycle progression and inducing apoptosis. *Food Chem Toxicol* 2006;**44**:704–13.
50. Shen KH, Chang JK, Hsu YL, Kuo PL. Chalcone arrests cell cycle progression and induces apoptosis through induction of mitochondrial pathway and inhibition of nuclear factor kappa B signalling in human bladder cancer cells. *Basic Clin Pharmacol Toxicol* 2007;**101**: 254–61.
51. Kitanosono Taku, Miyo Masumi, Kobayashi S. The combined use of cationic palladium(II) with a surfactant for the C–H functionalization of indoles and pyrroles in water. *Tetrahedron* 2015;**71**:7739–44.
52. Schrödinger. Schrödinger Suite. New York 2017: LLC, 2017. Available from: <https://www.schrodinger.com/releases/release-2017-4>.

53. Livak KJ, Schmittgen TD. Analysis of relative gene expression data using real-time quantitative PCR and the $2^{-\Delta\Delta CT}$ method. *Methods* 2001;**25**:402–8.
54. Oh YJ, Seo YH. A novel chalcone-based molecule, BDP inhibits MDA-MB-231 triple-negative breast cancer cell growth by suppressing Hsp90 function. *Oncol Rep* 2017;**38**:2343–50.
55. Martel-Frchet V, Kadri M, Boumendjel A, Ronot X. Structural requirement of arylindolylpropanones as anti-bladder carcinoma cells agents. *Bioorg Med Chem* 2011;**19**:6143–8.
56. Khan I, Garikapati KR, Setti A, Shaik AB, Kanth Makani VK, Shareef MA, et al. Design, synthesis, *in silico* pharmacokinetics prediction and biological evaluation of 1,4-dihydroindeno[1,2-*c*]pyrazole chalcone as EGFR/Akt pathway inhibitors. *Eur J Med Chem* 2019; **163**:636–48.
57. Gil HN, Jung E, Koh D, Lim Y, Lee YH, Shin SY. A synthetic chalcone derivative, 2-hydroxy-3',5,5'-trimethoxychalcone (DK-139), triggers reactive oxygen species-induced apoptosis independently of p53 in A549 lung cancer cells. *Chem Biol Interact* 2019;**298**: 72–9.
58. Cong H, Zhao X, Castle BT. An indole-chalcone inhibits multidrug-resistant cancer cell growth by targeting microtubules. *Mol Pharm* 2018;**15**:3892–900.
59. Macdonald A, Campbell DG, Toth R, McLauchlan H, Hastie CJ, Arthur JS. Pim kinases phosphorylate multiple sites on bad and promote 14-3-3 binding and dissociation from Bcl-XL. *BMC Cell Biol* 2006;**7**:1.
60. Zippo A, De Robertis A, Serafini R, Oliviero S. PIM1-dependent phosphorylation of histone H3 at serine 10 is required for MYC-dependent transcriptional activation and oncogenic transformation. *Nat Cell Biol* 2007;**9**:932–44.
61. Katoh M, Nakagama H. FGF receptors: cancer biology and therapeutics. *Med Res Rev* 2014;**34**:280–300.
62. Hu B, Mitra J, van den Heuvel S, Enders GH. S and G2 phase roles for Cdk2 revealed by inducible expression of a dominant-negative mutant in human cells. *Mol Cell Biol* 2001;**21**:2755–66.
63. Nava-Tapia DA, Cayetano-Salazar L, Herrera-Zúñiga LD, Bello-Martínez J, Mendoza-Catalán MA, Navarro-Tito N. Brazilin: biological activities and therapeutic potential in chronic degenerative diseases and cancer. *Pharmacol Res* 2022;**175**:106023.
64. Yuan H, Li ZM, Shao J, Ji WX, Xia W, Lu S. *FGF2/FGFR1* regulates autophagy in *FGFR1*-amplified non-small cell lung cancer cells. *J Exp Clin Cancer Res* 2017;**36**:72.
65. Lai Y, Wei X, Lin S, Qin L, Cheng L, Li P. Current status and perspectives of patient-derived xenograft models in cancer research. *J Hematol Oncol* 2017;**10**:106.